




Near-real-time ash cloud height estimation based on GOES-16 satellite imagery: a case study of the 2022–2023 eruption of Cotopaxi volcano, Ecuador

 Anais Vásconez Müller* ^α,  Benjamin Bernard^α, and  Francisco J. Vasconez^{α,β}

^α Instituto Geofísico, Escuela Politécnica Nacional, Quito, Ecuador.

^β University of Bristol, Earth Science Department, Bristol, UK.

ABSTRACT

Timely acquisition of ash cloud heights is crucial for aviation safety and forecasting volcanic ash dispersion and fallout. Since visual observations are not always available, we assess the suitability of retrieving ash cloud heights from brightness temperature and plume direction observed in GOES-16 satellite imagery, VOLCAT solutions, and Washington-VAAC advisories during the 2022–2023 eruption of Cotopaxi volcano, Ecuador. We find that these satellite-derived height estimates consistently yield lower values than visual cameras. While the plume direction method and Washington-VAAC advisories produce the closest approximations, they also exhibit significant deviations. Remarkably, the brightness temperature method, despite producing the lowest height values, shows the best linear regression with visual observations. Near-real-time retrieval of ash cloud height from GOES-16 imagery is a promising alternative to direct visual observation, particularly at night, in adverse weather, or for remote volcanoes, especially if improvements, such as incorporating high-resolution local meteorological models, are introduced.

RESUMEN

La estimación de la altura de columnas de ceniza es crucial para la seguridad aérea y predecir posibles áreas de afectación. Aquí evaluamos la prefactibilidad de estimar las alturas de nubes volcánicas a partir de su temperatura de brillo y dirección observadas en imágenes satelitales GOES-16, soluciones VOLCAT y avisos Washington-VAAC durante la erupción del volcán Cotopaxi 2022–2023. Al comparar, observamos que estas estimaciones satelitales son más bajas que las de las alturas observadas en cámaras visuales. La metodología de la dirección y avisos W-VAAC ofrecen promedios cercanos, pero también presentan desviaciones significativas. El método de temperatura de brillo, pese a producir los menores valores de altura, muestra la mejor correlación lineal con las observaciones visuales. En conclusión, la estimación de alturas de nubes de ceniza con imágenes GOES-16 es un método prometedor, especialmente en condiciones climáticas adversas o para volcanes remotos, sobre todo si se incorporan modelos meteorológicos locales.

KEYWORDS: Ash cloud height; Satellite imagery; GOES-16; Cotopaxi; VAAC.

1 INTRODUCTION

Ash column height is a crucial piece of information for quick hazard assessment during volcanic crises, especially since volcanic ash can pose a serious threat to aviation safety [Guffanti et al. 2010; Clarkson et al. 2016]. Volcanic ash can also have a negative impact on crops, livestock, and critical infrastructure [Wilson et al. 2012; Wilson et al. 2014; Blake et al. 2017; Osman et al. 2022; Ramírez et al. 2022; Ligot et al. 2023], and can even be detrimental to human health [Barsotti et al. 2010; Jenkins et al. 2015; Stewart et al. 2022]. While lower ash clouds usually cause fallouts in areas close to the volcanic center, higher ash plumes can travel further and affect larger areas [Cas and Wright 1996; Bonadonna et al. 2015]. Consequently, the correct assessment of ash cloud height is imperative for reliable ash dispersion and fallout forecasts [Folch et al. 2012; Scollo et al. 2019; Dioguardi et al. 2020]. Moreover, ash column height is a key input parameter used in empirical and statistical models to derive the mass eruption rate (MER) and, in combination, MER and column height are fundamental in the characterization of any explosive eruptive event [Mastin et al. 2009; Degruyter and Bonadonna 2012; Dioguardi et al. 2020;

Aubry et al. 2023; Mereu et al. 2023]. Ash cloud height estimation in near-real-time via satellite imagery is especially useful for volcano observatories when eruptions happen during the night, when cloudy weather makes it impossible to observe the eruption on camera, or when webcams are simply not available [Webley et al. 2009; Gordeev et al. 2016; Scollo et al. 2019].

At Cotopaxi volcano (5897 m, 0.677 °S, 78.436 °W), obtaining an accurate ash cloud height estimation in near-real-time is particularly valuable: its small (< 1 km above the crater) eruptive columns rarely cause ash fall outside the surrounding National Park (< 15 km); however, somewhat higher ash emissions have resulted in ash fallout in Ecuador's capital city of Quito, with 3 million inhabitants, which lies only 50 km to the north, and as far as the city of Manta, 250 km to the west [Bernard et al. 2016]. Historic records and tephrostratigraphy indicate that Cotopaxi has had 13 moderate-sized to large (VEI ≥ 3) eruptions in the past 500 years, with the last significant one taking place in 1877 [Sodiolo 1877; Barberi et al. 1995; Hall and Mothes 2008]. During the last decade, Cotopaxi has had two minor eruptive phases one in 2015 that lasted from August to November and expelled 1.2×10^9 kg of ash [Bernard et al. 2016], and a more recent one between October 2022 and July

*✉ avasconez@igepn.edu.ec

2023. The latter was characterized by ash emissions reaching between 0.1 and 3 km above crater level (acl) that lasted from minutes to days.

The objective of this manuscript is to evaluate the accuracy and usefulness of several satellite-based ash cloud height estimates when compared to plume heights observed via real-time webcams for Cotopaxi volcano between October 2022 and July 2023. These include heights obtained in near-real-time using the direction and brightness temperature of the ash emissions observed in images captured by the GOES-16 satellite, freely available on the NOAA/CIMSS website, in combination with READY global atmospheric models, as well as heights delivered by the VOLcanic Cloud Analysis Toolkit (VOLCAT) algorithms [Pavolonis et al. 2018; 2015a; 2015b] and reports from the Washington Volcanic Ash Advisory Centre (W-VAAC). Additionally, because of its high temporal resolution, the analysis of GOES-16 satellite imagery presented in this article allows for the timely and regular tracking of ash cloud direction, reach, and speed to aid ash dispersion and fallout forecasts.

2 DATA AND METHODS

2.1 Webcam ash column height estimates

Seven webcams register Cotopaxi's subaerial activity from different angles, distances, and visual fields (Figure 1A). Images are taken every one to five minutes during the 12 hours of daylight, while Sincholagua and Lasso webcams also capture images during nighttime. All webcam data are sent in real-time to the Instituto Geofísico de la Escuela Politécnica Nacional (IG-EPN) headquarters in Quito, where images are collected and analyzed. Sincholagua webcam, located 14 km north-northeast of Cotopaxi, is used here as a reference station since it captures images every minute (highest sampling frequency), works 24 hours a day (night mode), and the northeastern view is usually the clearest one (Figure 1B).

Since Cotopaxi's reactivation on 21 October 2022, images have been analyzed using stencil overlays like the one shown in Figure 1B, allowing quick retrieval of ash plume heights using Cotopaxi's summit as reference. Additionally, the overlays serve to approximate the dispersal direction of the ash clouds. Similar to the visible camera calibration described in Calvari et al. [2011] and Scollo et al. [2019], when elaborating the stencil overlays, we use known distances between distinct topographic features of the summit to calibrate the height scale for each camera. For accuracy, the height values are estimated vertically above the volcano, where the column falls inside or close to the superposed scale. Nonetheless, the stencils convey a variable geometric error, mostly due to the camera tilt, field of view, and distance to the vent, in addition to a reading error that is approximately half of the stencil scale interval (Table 1). Depending on plume orientation and visibility, images from various webcams are scrutinized to get a perpendicular view of the ash plume and assess its height as accurately as possible, assuming the plume is confined to a vertical plane. Some examples of ash emissions observed by various webcams are given in Supplementary Material 1, highlighting the importance of retrieving ash column height

Table 1: Characteristics of the seven webcams capturing Cotopaxi's superficial activity. The distance is measured between the camera and the vent, the maximum (max.) field vision describes the maximum plume height captured by each camera and the geometric (geom.) error was calculated at 1000 m acl for each camera. Nr. describes the number of times each camera was used to retrieve ash cloud height during the study period.

Name	Lat	Long	Altitude (m acl)	Distance (km)	Resolution (px)	Field of view (°)	Azimuth (°)	Tilt (°)	Max. field vision (m acl)	Geom. error (%)	Reading uncertainty (m)	Nr.
Sincholagua	-0.557	-78.409	3972	14.5	1024 × 768	23.4 × 19.9	195.4	5.35	2200	10.8	± 50	240
La Merced	-0.579	-78.41	3710	12.1	800 × 600	56.0 × 40.9	201.4	11.34	3100	11.7	± 50	13
Rumiñahui	-0.594	-78.467	4007	10.6	800 × 600	33.6 × 29.4	163.9	9.57	3400	22.8	± 50	9
Barranca Alta	-0.783	-78.475	3630	11.9	640 × 480	43.8 × 41.0	21.7	17.7	6000	0.2	± 100	5
Lasso	-0.752	-78.611	3008	21	800 × 600	20.5 × 14.8	71.3	8.47	3500	28.2	± 100	2
Tambo	-0.678	-78.399	4278	4.4	1280 × 720	119 × 62	266	13.56	2800	30.5	± 50	1
WIRA	-0.903	-78.723	3613	40.1	800 × 600	20.0 × 18.1	53.5	9.09	10500	-1.8	± 250	0

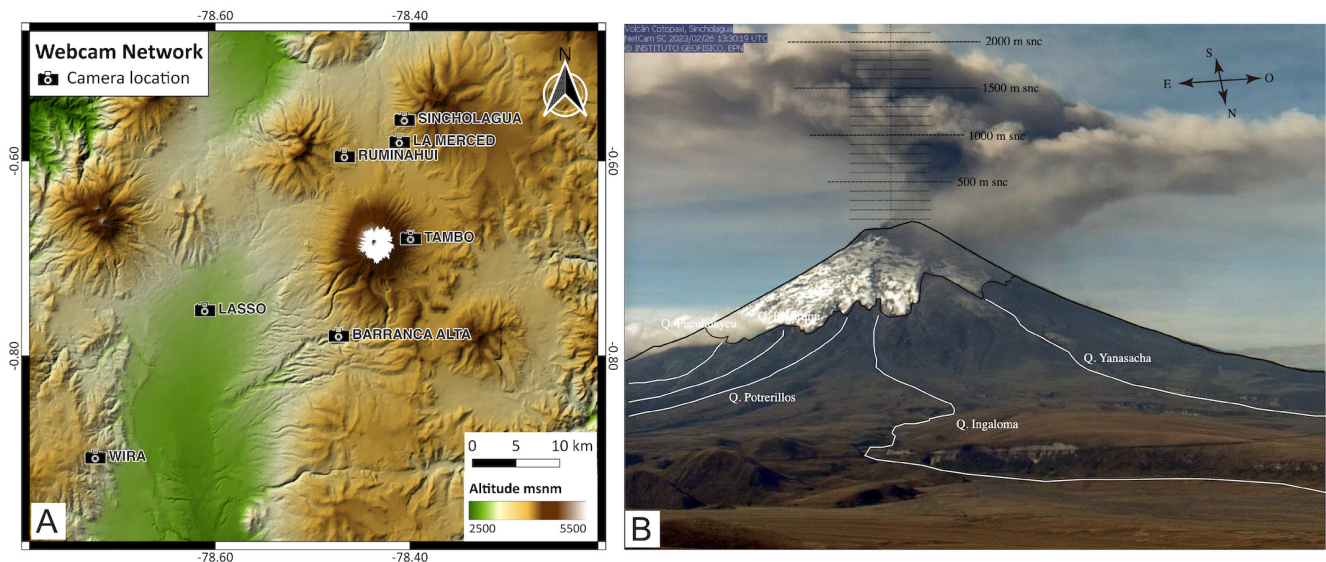


Figure 1: [A]: IG-EPN webcam network of Cotopaxi volcano. [B]: Ash emission at Cotopaxi on 26 February 2023 at 13:30 UTC captured by Sincholagua webcam with stencil overlay to estimate ash plume height and dispersal direction. Note that the ash cloud is directed towards the west below 1.5 km acl and towards the east up to 2.1 km acl.

from a webcam with a clear view perpendicular or opposite to the ash dispersion direction. In addition, the assembly of visual cameras located at different distances from the volcano facilitate capturing various ranges of plume heights (Table 1).

2.2 Volcanic cloud monitoring and measurements

In addition to webcams, satellite imagery allows for the detection and analysis of eruptive ash clouds. In this work, we use GOES-16 images processed by and provided on the NOAA/CIMSS Volcanic Cloud Monitoring portal*, summarized in Table 2. These pre-processed images in the channels readily available on the Volcanic Cloud Monitoring portal are used instead of raw ones due to the reduced time invested in obtaining and treating the data, which is especially useful for volcano observatories during 24/7 monitoring activities.

Specifically, we use RGB-85 and BT-D imagery to visually distinguish volcanic ash emissions (Table 2, Figure 2A). The Volcanic Cloud Imagery web interface also allows the retrieval of the coordinates and, thus, the direction and reach of the scrutinized ash emissions with the tools Draw Points and Save Points. These coordinates are referential, as the 2 km-wide pixel size of GOES-16 satellite imagery, as well as the subjectiveness of selecting the endpoint of the ash emission, will influence the precision of the resulting values.

BT Color Enhanced Infrared Imagery is used to retrieve the brightness temperature (T) of the ash clouds in Kelvin (K). To do this, the color of the pixels corresponding to the ash emission are compared to those shown in the legend at the bottom (Figure 2B). Here, the most opaque pixels are selected to avoid the contribution of warmer radiation from below mixing into the brightness temperature signature of the ash cloud [Bailey et al. 2010; Scollo et al. 2019; Guerrieri et al. 2023]. To match the color of the emission precisely to the brightness temperature, these images can be analyzed in an image ma-

nipulation software that has the tool “select by color”, such as GIMP†. According to Scollo et al. [2019] and Guerrieri et al. [2023], an uncertainty of ± 2 K can be assumed when retrieving the brightness temperature, resulting in a height error of up to ± 500 m, depending on the temperature gradient of the atmosphere.

2.2.1 Global meteorology data

To estimate the height of the ash emissions based on their direction and brightness temperature we use the Real-time Environmental Applications and Display sYstem (READY) developed by the Air Resources Laboratory of NOAA‡ [Rolph et al. 2017]. We use the Sounding of Current & Forecast Meteorology (GFS Model 1 deg, 0-240 h, 3 hrly, Global, pressure) to obtain modeled wind data during eruptions and estimate plume height and speed, and later use Archived Meteorology Sounding (GDAS 1 deg, 3 hrly, Global) data to confirm or correct them (Figure 3).

2.2.2 Calculations

A total of 168 ash emissions of varying size and duration were detected by IG-EPN’s camera monitoring network during the last eruptive phase of Cotopaxi volcano between October 2022 and July 2023. For the 62 largest ash emissions that were clearly observed on GOES-16 satellite imagery, the subsequent calculations were performed at least once to obtain their direction, reach, brightness temperature and consequent estimated height and speed at one point in time.

To calculate the height of an ash cloud based on its brightness temperature, we apply the following formula:

$$H = H_1 + \frac{(H_2 - H_1) * (T - T_1)}{(T_2 - T_1)} \quad (1)$$

†<https://www.gimp.org/>

‡<https://www.ready.noaa.gov/READYamet.php>

*<https://volcano.ssec.wisc.edu/imagery/view/>

Table 2: Image types available on the NOAA/CIMSS Volcanic Cloud Monitoring portal and corresponding GOES-16 band combinations. The abbreviations given here are used hereinafter when referring to the different image types.

Image type	Channel name	Band combinations	Description	Abbreviation
BT11um	Color Enhanced Infrared Imagery	10.3 μm	Shows brightness temperature in Kelvin (K)	BT
BTD1112um	Split-Window Imagery	12.3–10.3 μm	Shows brightness temperature difference (BTD) in Kelvin (K)	BTD
REF065um	Visible Imagery	0.64 μm	Shows reflectance in percent (%)	REF
RGB1112or13um 3911um 11um	False Color Imagery	12.3–10.3 μm , 10.3–3.9 μm , 10.3 μm	Best shows gas-rich emissions	RGB-39
RGB1112um 8511um 11um	False Color Imagery	12.3–10.3 μm , 10.3–8.5 μm , 10.3 μm	Best shows ash-rich emissions	RGB-85
Ash Height	IR Window Imagery and Ash/Dust Cloud Height	10.3 μm underlay / VOLCAT algorithm	Shows the ash cloud height in km asl ONLY for ash clouds detected by VOLCAT	Ash Height
Ash Loading	IR Window Imagery and Ash Loading	10.3 μm underlay / VOLCAT algorithm	Shows the ash loading in g m^{-2} ONLY for ash clouds are detected by VOLCAT	Ash Load
Ash Probability	IR Window Imagery and Ash Probability	10.3 μm underlay / VOLCAT algorithm	Shows the probability of areas detected by VOLCAT to contain ash/dust particles in %	Ash Prob
Ash Reff	IR Window Imagery and Ash/Dust Effective Radius	10.3 μm underlay / VOLCAT algorithm	Shows the effective radius of ash particles in μm ONLY for ash clouds are detected by VOLCAT	Ash Reff

where T is the brightness temperature of the ash emission that we obtain from the Color Enhanced Infrared Imagery (e.g. -9°C in Figure 2B), T_1 and T_2 are the temperatures given in the READY Sounding product that encompass T (e.g. -8.9°C and -16.5°C in Figure 3), and H_1 and H_2 are the heights in meters above sea level corresponding to T_1 and T_2 , respectively (e.g. 6692 and 7589 m asl in Figure 3). Importantly, since the temperature values reported in the READY output files are given in degrees Celsius, the brightness temperature values obtained from the Color Enhanced Infrared Imagery Images must first be transformed from Kelvin to Celsius. Generally, the pixel color that indicates the lowest brightness temperature is chosen to estimate the maximum ash cloud height [see Bailey et al. 2010; Scollo et al. 2019]. In the present example, the brightness temperature T of -9°C corresponds to a height of 6704 m asl (807 m acl).

The same procedure is applied to estimate the ash column height based on the direction of the ash plume by replacing the temperature variable with that of direction:

$$H = H_1 + \frac{(H_2 - H_1) * (D - D_1)}{(D_2 - D_1)}. \quad (2)$$

Here, the direction D of the ash emission can previously be calculated based on the coordinates of the volcano (lat = Y_1 , long = X_1) and those of the furthest point of the ash emission (lat = Y_2 , long = X_2 ; arrowhead in Figure 2A) in decimal degrees as follows:

$$D = 90 - \text{atan} \frac{Y_1 - Y_2}{X_1 - X_2}, \quad (3)$$

which applies when the ash emission is directed between north and south towards the west. If the wind blows towards the east, the formula changes slightly to:

$$D = 270 - \text{atan} \frac{Y_1 - Y_2}{X_1 - X_2}. \quad (4)$$

In Equation 2, D_1 and D_2 are the direction values that enclose D in the READY Sounding product, and H_1 and H_2 are the heights in meters above sea level corresponding to D_1 and D_2 , respectively. In the example of Figure 2A, after applying equation (4), a wind direction of N297 results for the ash cloud observed to disperse to the southeast. As shown in Figure 3, in this case, the direction of the ash emission is not encompassed by any two wind direction values reported in the GDAS Sounding wind files. Considering that the coordinates and the resulting direction values are subject to imprecisions, wind directions that fall within 25 degrees of the manually retrieved values can be used to estimate ash cloud height. Here, for example, the wind direction of N275.2 and the corresponding height of 7589 m asl (1692 m acl) was used (Figure 3). When none of the wind directions reported in the READY Sounding files fall close to the observed direction, this method cannot be used to estimate ash cloud height.

To calculate the reach (R) of the ash cloud, we use the haversine formula:

$$R = 2r \text{asin} \left(\sqrt{\sin^2 \left(\frac{Y_1 - Y_2}{2} \right) + \cos \cos(Y_1) \times \cos \cos(Y_2) \times \sin^2 \left(\frac{X_1 - X_2}{2} \right)} \right), \quad (5)$$

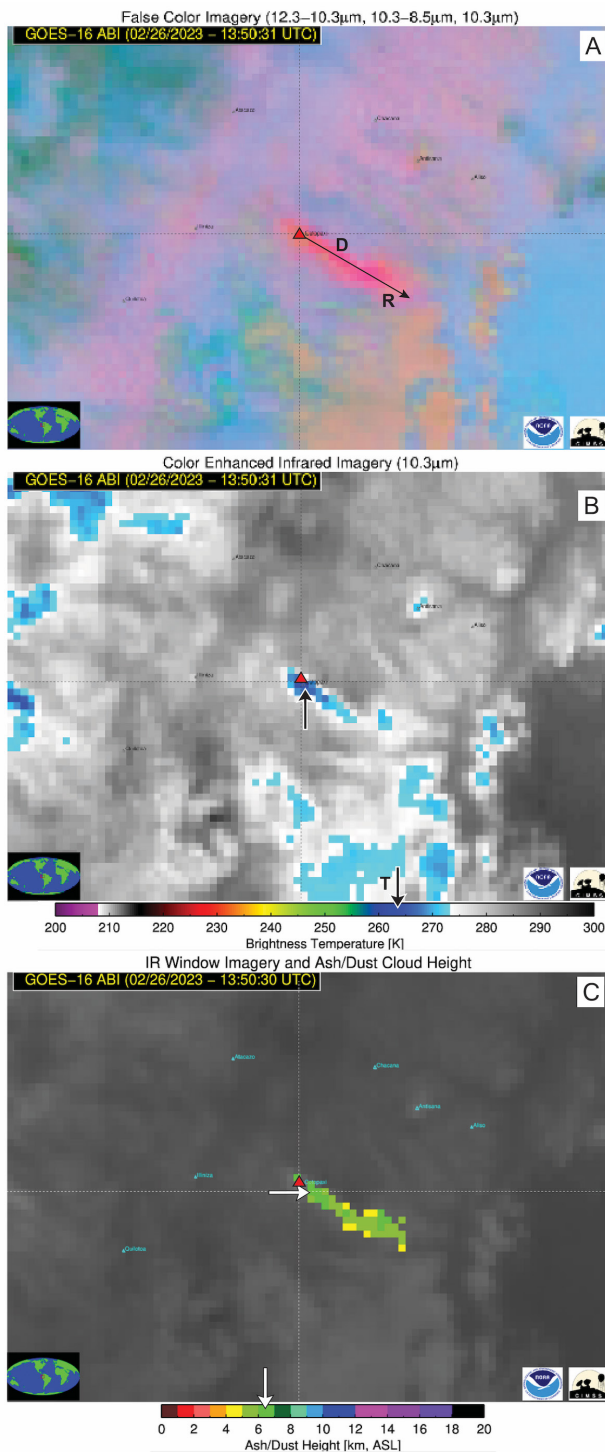


Figure 2: Ash emission at Cotopaxi on 26 February 2023 at 13:50 UTC captured by GOES-16 satellite imagery. [A] RGB-85 imagery with the main direction D and reach R of the ash cloud indicated by the black arrow. [B] BT imagery, the black arrows point to the pixel color that indicates the lowest brightness temperature T of 264 K ($-9\text{ }^{\circ}\text{C}$). [C] Ash Height between 6 and 7 km asl (0.1–1.1 km acl) suggested by the VOLCAT algorithm, as indicated by the white arrows. Note that, similar to Figure 1, the ash cloud moves mostly to the southeast and a minor portion to the northwest.

```
gdas1.feb23.w4
Lat/Lon: -0.68 -78.44
E = Estimated Surface Height

=====Mean Sea Level Pressure=====
FHR: 0.
MSLP: 1017.

==Temperature Deg C==           ==Wind Direction==           ==Wind Speed m/s==
Hms1/FHR: 0.                    Hms1/FHR: 0.                 Hms1/FHR: 0.
Mdl sfc 12.7                    2130. 61.0                   2130. 0.2
2130. 12.7                      2579. 79.1                   2579. 1.3
2579. 11.2                      3151. 58.5                   3151. 1.2
3151. 8.3                       3761. 86.9                   3761. 1.7
3761. 5.6                       4412. 126.1                  4412. 2.1
4412. 2.5                       5112. 134.0                  5112. 2.8
5112. -0.5                      5868. 122.3                  5868. 2.7
5868. -3.7                      6692. 230.0                  6692.H1 1.1 S1
6692.H1 -8.9 T1                 7589.H1 275.2 D1             7589.H2 4.6 S2
7589.H2 -16.5 T2                8578. 272.8                  8578. 6.8
8578. -23.4                     9686. 115.1                  9686. 9.1
9686. -32.1                    10945. 104.1                 10945. 9.4
10945. -41.9                   12417. 129.9                 12417. 7.7
12417. -54.1                   14199. 244.8                 14199. 2.3
14199. -67.4                   16542. 337.4                 16542. 2.5
16542. -84.0                   20523. 285.2                 20523. 14.3
20523. -65.5                   26201. 248.6                 26201. 10.1
26201. -59.0
```

Figure 3: READY Archived Meteorology Sounding GDAS product for 26 February 2023, 12 UTC for Cotopaxi's coordinates. Note the direction shift between 5868 and 7589 m asl (0 and 1.7 km acl) from NW to E, which corresponds approximately to the ash cloud directions in both the visual camera (Figure 1B) and the satellite imagery (Figure 2). Marked values are used to exemplify the variables of the calculations presented in the following section, where T1 ($-8.9\text{ }^{\circ}\text{C}$) and T2 ($-16.5\text{ }^{\circ}\text{C}$) encompass the brightness temperature of $-9\text{ }^{\circ}\text{C}$ retrieved in Figure 2B, and D1 (N275.2) is the direction value that comes closest to the observed main dispersal direction (N297 in Figure 1A).

where r is the Earth's radius (6378.134 km at Cotopaxi). The error of using the haversine formula for a non-spherical object is much smaller than the error of manually drawing the ash cloud coordinates in the Volcanic Cloud Monitoring interface. Applying this formula to the ash cloud observed on Figure 2A we obtain an approximate reach of 35 km.

Once we have obtained the heights estimated via temperature and/or direction of the ash emission, we can use the READY Sounding data to estimate the wind speed at said height:

$$S = S_1 + \frac{(S_2 - S_1) * (H - H_1)}{(H_2 - H_1)} \quad (6)$$

so that H is the height we calculated with either method, H_1 and H_2 are the heights encompassing H on the READY output, and S_1 and S_2 are the wind speeds corresponding to H_1 and H_2 (Figure 3). In the present example, the height estimated based on the brightness temperature yields a speed of 1.1 m s^{-1} and that of the direction method 4.6 m s^{-1} .

For long-lasting ash emissions, these calculations were performed more than ten times to track the evolution of the aforementioned parameters over time. Importantly, these calculations were performed initially with the forecasted global meteorology models (GFS), to obtain preliminary results, and later repeated with archived global meteorology data (GDAS) to confirm or correct the height and speed estimates. A spreadsheet containing the above formulas with the example of Cotopaxi can be found as Supplementary Material 2. This spreadsheet can be easily modified to be used at other volca-

noes by replacing the volcano coordinates, height, and Earth's radius with the desired data.

2.3 Washington Volcanic Ash Advisory Center

Satellite imagery and global forecast meteorological models are also used by the Washington Volcanic Ash Advisory Center, which is part of the National Environmental Satellite, Data, and Information Service (NESDIS) and the Satellite Analysis Branch's (SAB) Volcanic Ash Program, to issue ash advisories that include ash cloud height, direction, and speed (Figure 4). The ash cloud characteristics reported in the advisories can be based on a combination of various sources, such as: webcam observations, local Volcano Observatory Notices for Aviation (VONAs), reports by Meteorological Watch Offices (MWOs), pilot reports, VOLCAT outputs, as well as false color and infrared satellite imagery paired with numerical weather prediction models [Beckett et al. 2024]. Between October 2022 and July 2023, the W-VAAC issued 186 volcanic ash advisories for ash emissions observed at Cotopaxi. The heights, reported in FL (flight level) are transformed to m asl and m acl.

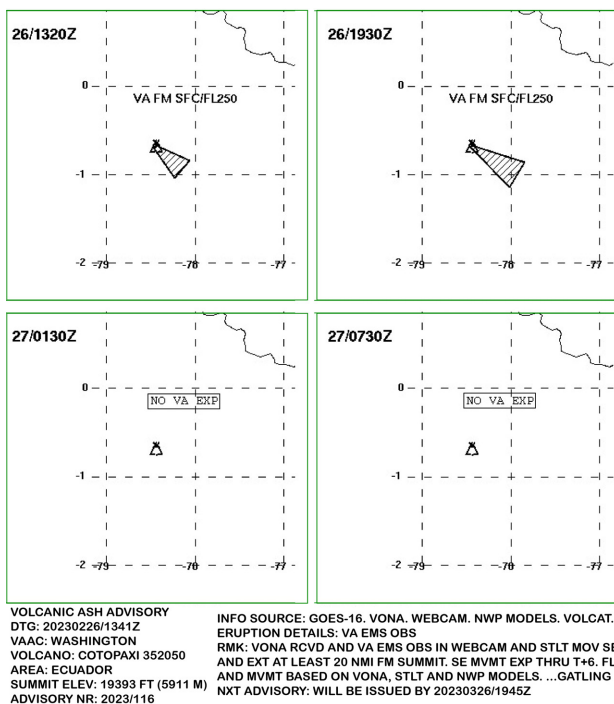


Figure 4: W-VAAC Alert Number 116 for Cotopaxi issued on 26 February 2023 at 13:20 UTC. Note that only the main dispersal direction is indicated and that the flight altitude (FL250 = 7620 m asl = 1709 m acl) is similar to the value obtained with the direction method and lower than the webcam estimate.

3 RESULTS

3.1 Height estimation through webcams

During the latest eruptive phase of Cotopaxi, 270 ash plume height values were obtained via direct webcam observations. As reported in Table 3 and displayed in Figure 5A, the maximum ash column height observed at Cotopaxi during this eruptive period was 3 km acl in January, February, and March

2023. Due to weather conditions, sometimes the ash plume was observed to “boil over” and descend along Cotopaxi's flanks. In such cases, the height closest to the crater was measured. Generally, during clear-sky conditions, these types of emissions were registered with low positive heights (100–300 m) above the summit before descending. However, in rare cases when the summit was clouded but the ash plumes were observed descending along the flanks, we recorded heights below the crater. Since our stencil overlays use Cotopaxi's summit as reference height (0 m acl), they were assigned negative height values, with a minimum of –500 m registered on cameras in February. On average, ash plumes reached a height of 1171 m acl, with a standard deviation of 655 m.

3.2 Height estimation through satellite imagery

Between October 2022 and July 2023, 127 ash cloud heights were estimated based on the direction of the ash emissions observed in GOES-16 satellite imagery. In 38 of those cases, the GFS model was used to calculate a preliminary height, before obtaining the archived GDAS data and calculating the final one. Similarly, 137 heights were obtained based on the brightness temperature of the ash clouds, of which in 44 cases the GFS was used before GDAS data was available. When estimates fall below Cotopaxi's height (5897 m asl), these are reported as negative values or in meters below crater level (bcl). As visualized in Figure 5B and summarized in Table 3, the direction method yielded a maximum height of 3220 m acl and a minimum of 1259 m bcl, while the maximum and minimum ash cloud height estimates obtained from the brightness temperature were 2692 m acl and 1800 m bcl, respectively.

For 98 of the height estimates performed by applying the calculations presented above, VOLCAT height estimates were also available, registering a maximum of 2103 m acl and a minimum of 1397 m bcl, as depicted in Figure 5C and summarized in Table 3. The 186 advisories issued by the Washington VAAC, on the other hand, on principle report only positive heights, with a maximum of 3233 m acl and a minimum of 185 m acl.

Regarding the median values, the lowest heights were obtained via the temperature in combination with GDAS and GFS (252 and 331 m acl, respectively), followed by the direction with GDAS data (558 m acl), VOLCAT products (603 m acl), the direction with GFS data (638 m acl), and W-AAC advisories (795 m acl). In comparison, the median height observed on webcams was 1100 m acl (Table 3, Figure 5).

3.3 Height comparison

Here, we consider ash column heights observed via webcam to be the most reliable estimates, thanks to a combination of factors, such as their lowest ground sampling distance, highest temporal resolution, and least amount of assumptions. Building on this argument, as well as the fact that webcam observations are commonly used at volcano observatories for timely hazard communication, we compare them to height estimates obtained from satellite imagery analysis. We compute the linear regression equations ($f(x) = ax + b$) and the coefficient of determination (R^2) for each comparison in order to assess the correlation of the different height sources with the visual

Table 3: Statistical parameters for the seven ash cloud height sources. Count of measured heights (Nr.), maximum (max), minimum (min), median (md), mean, and standard deviation (stdev) in meters above crater level. Negative values indicate ash emission heights below the crater.

Source	Nr.	max	min	md	mean	stdev
Webcams	270	3000	−500	1100	1171	655
Direction GFS	38	2689	−359	638	847	783
Direction GDAS	126	3220	−1259	558	763	829
Temperature GFS	43	2692	−1317	331	409	804
Temperature GDAS	136	2692	−1800	252	240	740
VOLCAT	97	2103	−1397	603	711	701
W-VAAC	186	3233	185	795	911	478

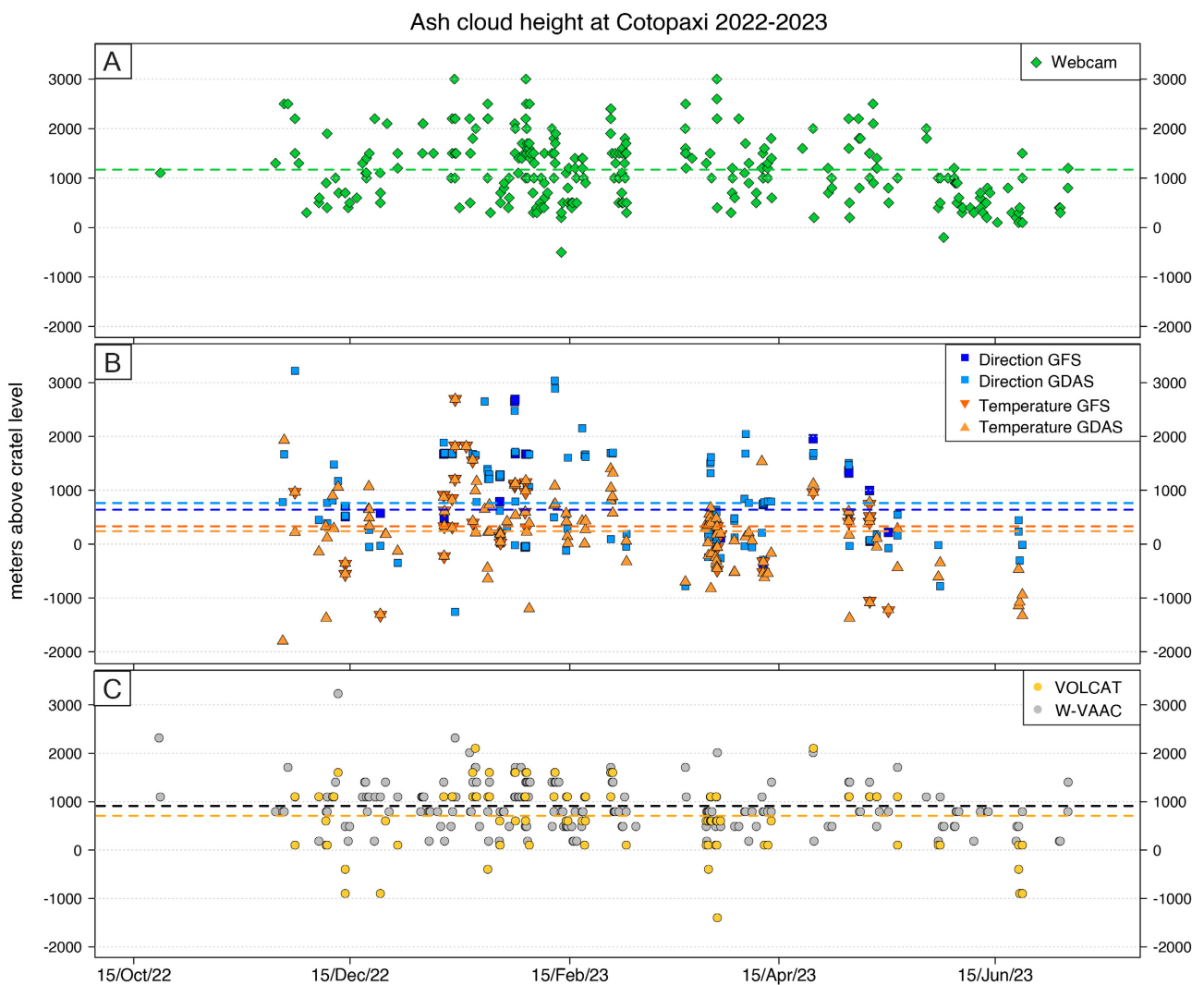


Figure 5: Ash column height as [A] observed on IG-EPN's webcams, [B] obtained based on the direction and brightness temperature in combination with global GFS and GDAS atmospheric models, and [C] retrieved from VOLCAT outputs and W-VAAC reports for Cotopaxi's ash emissions between October 2022 and July 2023. Dashed lines indicate the median values for each height source.

observations (Figure 6). A good correlation should have $a \approx 1$, $b \approx 0$ and $R^2 \approx 1$. Linear regression equations and R^2 computed for all methods when plotted against each other are compiled in Supplementary Material 3.

In 73 cases, when heights were estimated based on the direction of the ash clouds in combination with the archived meteorology data (GDAS), visually observed ash column heights were also available. Additionally, on 26 occasions heights

were estimated with the forecasted GFS models. As shown in Figure 6A, a wide scatter and weak correlation appears when these height estimates are compared to direct visual observations (R^2 of 0.36 and 0.17 for GFS and GDAS, respectively). Also, the origin values (b -values) are negative (-119 and -36 m for GFS and GDAS, respectively) and the slopes (a -values) are intermediate (0.75 and 0.54 for GFS and GDAS, respectively).

The height estimates obtained based on the brightness temperature of the ash clouds in combination with the forecasted (30) and archived (80) global meteorology models present a slightly better correlation (R^2 of 0.39 and 0.32, respectively) and also higher slopes (a -values of 0.85 and 0.7 for GFS and GDAS, respectively), when compared to the corresponding ash emission heights observed via webcam (Figure 6B). However, it is also the method with the lowest b -values of -822 and -810 m for GFS and GDAS, respectively.

As shown in Figure 6C, two of the weakest correlations result between webcam-derived heights and those retrieved from 59 VOLCAT outputs and 106 W-VAAC advisories (R^2 of 0.26 and 0.30, respectively). The poor regression quality is partly due to VOLCAT heights being retrieved from the legend in 500 m intervals, while W-VAAC heights are given in 1000 ft ($= 304.8$ m) steps. The linear regression fitted to the W-VAAC vs. visual observations is the only one with a positive b -value of 443 m, resulting in the lowest slope of all methods (a -value $= 0.39$).

Overall, all comparisons have an R^2 lower than 0.4, which indicates poor linear correlation, a -values < 1 , and mostly negative b -values, indicating that the various satellite imagery sources generally yield lower heights than webcam observations.

Figure 7 shows the difference between the heights obtained through applying the various methods and the heights observed on webcam for the same dates and times. Clearly, while all sources generally fall below visually estimated ash cloud heights, the temperature-method yields the lowest height estimates (GFS $Md = -1078$ m, GDAS $Md = -1218$ m). Conversely, on average, W-VAAC alerts are the closest to the visually observed heights ($Md = -213$ m). The largest deviations indicated by the whiskers range from -2660 m for the heights estimated from the temperature method to 819 m for W-VAAC reports.

4 DISCUSSION

4.1 Limitations

The main shortcoming of using satellite imagery to obtain key information about ash emissions, such as their height, is the delay with which satellite images are available. GOES-16 images, which are the ones used here, are taken every 10 minutes with a general delay of 20 to 30 minutes. Therefore, height estimations performed using this information are not in real-time. In operational terms, from the various methods presented here, VOLCAT outputs are available the fastest, since they are accessible as soon as GOES-16 imagery is published on the Volcanic Cloud Monitoring web interface. Retrieving the ash cloud height manually from satellite imagery via the direction

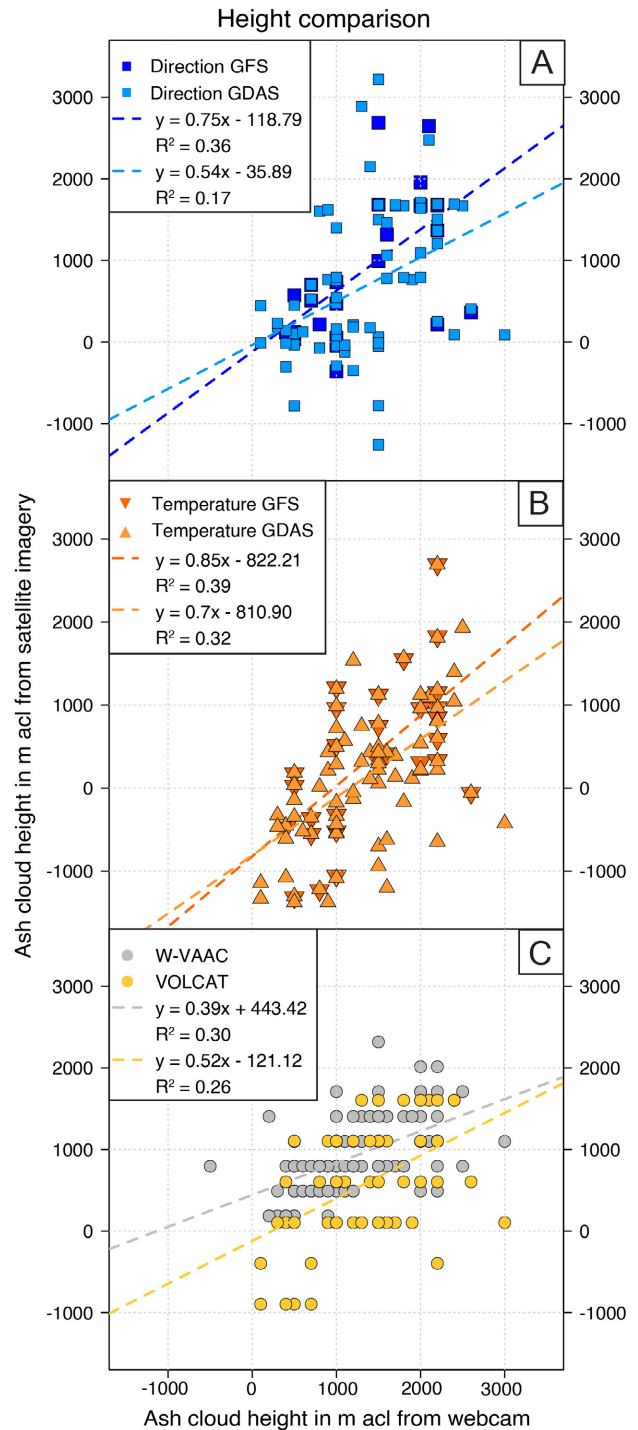


Figure 6: Comparison of ash column heights observed on webcam and heights estimated based on [A] the direction (GFS: 26, GDAS: 73) and [B] brightness temperature (GFS: 30, GDAS: 80) of the ash emissions, as well as [C] heights obtained from 59 VOLCAT products and 106 W-VAAC advisories.

and brightness temperature methods takes an additional 5 to 7 minutes. Similarly, the Washington VAAC generally issues its alerts within 30 minutes after an ash cloud observation. Nevertheless, having an ash cloud height estimate within 30 to 40 minutes of an eruption, along with spreading direction and speed, is highly valuable for hazard communication, es-

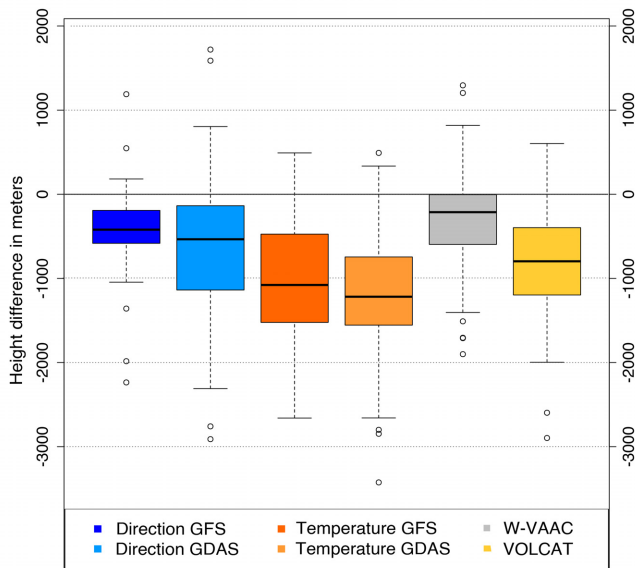


Figure 7: Boxplot depicting the height difference between the values obtained through the satellite imagery-derived methods and the heights observed on webcams for Cotopaxi volcano between October 2022 and July 2023.

pecially to warn larger towns and cities located further than 30 km away from the volcano. Additionally, ash particles, especially fine ones, take longer to settle [Bonadonna et al. 2015], which is why there is a delay between the observation of an ash cloud above a specific location and the first ash fall report at that place. Therefore, despite the delay with respect to direct visual observations, the use of satellite imagery to advise of likely ash fall has proven useful. However, for aviation safety, real-time visual observation and reporting of volcanic eruptions are more effective than relying on delayed reports derived from satellite imagery [Simpson et al. 2001].

Moreover, when dense meteoric clouds obscure the area of interest, ash emissions can be just as unobservable on satellite imagery as they are on webcams. Nevertheless, large eruptive plumes that can cause significant regional ash fall tend to surpass the meteoric cloud cover and can therefore be observed and analyzed on satellite imagery [Bailey et al. 2010; Pavolonis et al. 2018]. Importantly, as noted before by Simpson et al. [2000] and Tupper et al. [2007], moist atmospheric conditions—especially in tropical and subtropical areas—result in significant entrainment of atmospheric water vapor into high eruptive columns, with moisture masking the presence of volcanic ash. Therefore, in Ecuador, high ash clouds often take the color of meteoric ones in GOES-16 satellite imagery and are frequently missed by the VOLCAT algorithms, especially if they initially form beneath meteorological clouds [Pavolonis et al. 2018]. It is also mentioned by Pavolonis et al. [2015b] that one of the algorithms does not recognize portions of ash clouds that overlap low meteorological clouds. This is also observed in the case of weak ash plumes, where neither the vertical cloud growth, the optical depth, nor the contrast in brightness temperature with the clear sky is large enough to be easily detected by the automated VOLCAT algorithms. Hence the importance of manual analysis methods such as those based on

the direction and brightness temperature of ash clouds, so that expert personnel can rapidly assess and communicate the hazard posed by an eruption by visually distinguishing ash clouds on satellite imagery.

The estimation of ash cloud height using the emission's direction and brightness temperature is also limited by its dependence on global atmospheric models, which can be imprecise at the local scale, as evidenced by the frequent deviations between visually observed heights and directions and those presented in the READY Sounding files. The delay in the release of the archived meteorological data (>4 h) introduces an additional constraint on the confidence that can be placed in the results obtained based on the forecasted wind models, especially concerning the variable wind direction as a function of altitude. Inconsistency between predicted atmospheric data and visual observations is also occasionally remarked by the Washington VAAC in their advisories. Along the same lines, Bernard et al. [2022] noted that the azimuth of ash fallout in the field differed 10–20 degrees from that of the ash dispersion and deposition simulations of the Ash3D numerical model that runs on the GFS wind files [Mastin et al. 2013] during the 20 September 2020 eruption of Sangay, Ecuador. Possibly, the implementation of local, high-resolution atmospheric models could resolve this limitation and improve the height values obtained with the methods presented in this article.

Finally, the fact that we use processed satellite imagery to retrieve the brightness temperature adds a possible error of up to ± 2 K and, thus, up to ± 500 m in the heights calculated from that information [Scollo et al. 2019]. While this uncertainty could be reduced by using original GOES-16 imagery, the additional time and expertise needed to obtain and process that raw data would counteract the current aim of the height estimation methodology presented here, which is its rapid and simple implementation to issue timely warnings at volcano observatories. Additionally, uncertainties of 500 m are commonly assumed in various other ash cloud height estimation methods [e.g. Folch et al. 2012; Mastin 2014; Scollo et al. 2019; Dioguardi et al. 2020] and similar recent approaches that retrieve BT directly from raw satellite imagery still consider a height uncertainty of ± 300 m for this method [Guerreri et al. 2023]. Nevertheless, future work should examine the feasibility of implementing the continuous download, storage, processing and analysis of raw GOES-16 data for the characterization of volcanic ash emissions at volcano observatories.

4.2 Accuracy analysis

It is worth noting that recent studies, such as the one by Barnie et al. [2023] and Snee et al. [2023], underscore the importance of accounting for the influence of wind on the position and height of ash plumes in visual imagery. Fortunately, in the context of Cotopaxi, the presence of various webcams positioned around the edifice enables us to have azimuthal coverage and virtually always obtain a perpendicular perspective to the ash plume dispersion. This proves instrumental in more accurately evaluating ash column height and dispersal direction when visual conditions allow for it. Specifically, ash plume heights are retrieved from webcam imagery solely vertically above the volcanic edifice where they fall inside the super-

posed scale that was calibrated based on topographic features of the summit. As mentioned before, this method induces a fixed error related to the scale intervals, as well as a geometric error related to the camera tilt, field of view and distance to the vent of each camera. For the median height values registered on camera during the 2022–2023 eruptive phase of Cotopaxi (1100 m acl), the fixed plus the geometric uncertainty amount to ~160 and ~170 m for Sincholagua and La Merced webcams, respectively, which were used for 94 % of the height retrievals (Table 1). Uncertainties of this magnitude fall below those described in the literature for other calibrated visible cameras [e.g. Scollo et al. 2019; Barnie et al. 2023]. In addition, this is the most reliable, direct, and fastest method to observe and characterize ash emissions, and regardless of the inherent uncertainty, allows effective communication of the hazard level. Therefore, the aim of comparing ash cloud height estimates retrieved from satellite imagery to webcam heights is to evaluate their similarity and hence the possibility to use the former when the latter are unavailable.

Our study shows that the ash cloud height estimates obtained for Cotopaxi by all four satellite-based methods generally fall below those observed on webcam. It is important to note that the heights measured via camera correspond to maximum plume height values observed vertically above the volcano. In contrast, the 2 km-wide pixel size of the GOES-16 satellite imagery represents the average height of the larger-scale ash dispersion. This is exemplified by those ash plumes observed to descend along Cotopaxi's flanks, spreading at much lower heights than the height at which they were emitted. In Aubry et al. [2023] it is mentioned that spreading heights are predicted to reach only 76 % of the top column height, which could, in part, explain the lower values retrieved from satellite imagery when compared to visually obtained heights, in addition to the possible overestimation resulting from webcam readings due to the geometric scaling error.

Furthermore, concerning the brightness temperature method, for which the lowest ash cloud height estimates were obtained, previous studies such as Bailey et al. [2010], Scollo et al. [2019], and Guerrieri et al. [2023] state that a temperature overestimation and consequent height underestimation can arise from the combination between the temperature of the ash cloud and that of the underlying much warmer ground captured in satellite imagery. This temperature mixture occurs in the pixels along the edges of ash emissions and when ash clouds are partially translucent, highlighting the importance of selecting opaque, centered pixels close to the volcano. Thus, narrow ash plumes detected only in a few pixels and those with low ash content appear warmer in GOES-16 BT imagery and, consequently, yield lower heights. This applies to at least half of the ash emissions analyzed in the present case study, which were generally faint and dispersed quickly in the atmosphere. Even though we analyzed only those images in which the ash clouds could be clearly distinguished, the reduced extent of most ash emissions can primarily account for the low height estimates reported in this study. However, this also implies that the accuracy of this method increases for larger, wider, and more opaque ash clouds associated with

more explosive eruptions than those observed at Cotopaxi between October 2022 and July 2023. In addition, of the four analyzed satellite-based height sources, the brightness temperature method presents the best linear regression when compared to the visually obtained heights. Therefore, even if underestimated to a certain degree, height estimates based on the brightness temperature of ash clouds are useful to discriminate between small low-impact and moderate to large ash emissions, that should be notified immediately to the risk management agencies. To counteract the underestimation by the non-opacity of the pixels, future applications of this method could decrease the obtained BT by 2 K, as suggested by Prata and Grant [2001] and implemented by Corradini et al. [2016] and Guerrieri et al. [2023].

Regarding the broad scatter and consequent low coefficient of determination values observed for all four satellite-based ash cloud height sources when compared to visually obtained plume heights, it is noteworthy that other plume height estimation methods such as ground-based radar have been found to have a similar error ranging between <500 m and 2000 m depending on distance and beam width [e.g. Folch et al. 2012; Mastin 2014; Dioguardi et al. 2020; Marzano et al. 2020; Mereu et al. 2023]. Moreover, the various ash cloud height estimation methods performed at Etna volcano (Italy) by Corradini et al. [2016] and Guerrieri et al. [2023] also assume errors of 400 m (SEVIRI-Radar parallax), 800 m (SEVIRI-MODIS parallax), 300 m (darkest pixel), 700 m (cloud tracking), and 500 m (Hysplit method), while VONA column height uncertainty is set to 500 m. In addition, temporal variations in plume height due to internal (e.g. eruption intensity) and external (e.g. wind speed) factors further complicate the precise estimation of volcanic ash cloud height [Mastin 2014].

The scatter is particularly wide for the direction method, which depends strongly on the accuracy of global wind model data provided by the READY system, especially the Current & Forecast Meteorology, which is used to obtain the first height estimates of recently initiated eruptions. As shown in Figure 8, when comparing the deviation between the forecasted and the archived meteorological data from GFS and GDAS Soundings obtained from READY between March and August 2023 for Cotopaxi's coordinates, variations in wind direction of up to 50 degrees appear, while temperature variations stay within one degree. Additionally, as opposed to the atmospheric temperature gradient, wind direction changes rapidly and inconsistently with altitude, often resulting in more than one possible height that would match the observed spreading direction of the ash cloud. Nevertheless, in combination with the brightness temperature height estimate, which can serve as a guide when deciding which input values to use for the direction-height calculation, both estimates can help to evaluate and track the hazard level in near-real-time. When available, the VOLCAT outputs should additionally be considered to evaluate the likelihood of the height estimates [Bernard et al. 2022; Hidalgo et al. 2022]. The interquartile range, shown for each method in Figure 7, could possibly serve as a height uncertainty range when webcam images are not available.

On average, the height estimates reported by the W-VAAC fall the closest to the visually observed ash cloud heights at Co-

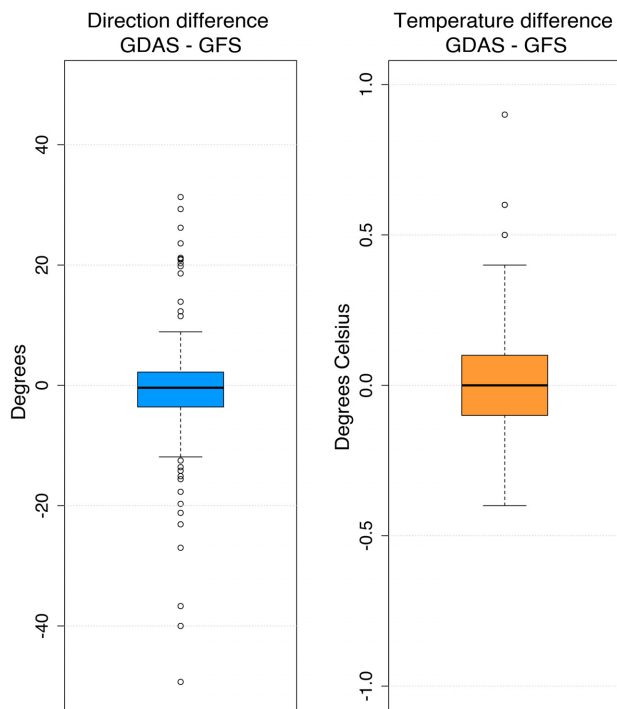


Figure 8: Boxplots showing variation between forecasted (GFS) and archived (GDAS) meteorological data provided by READY for Cotopaxi's coordinates between March and August 2023.

topaxi during this last eruptive phase. This can be ascribed to the fact that ash cloud heights reported in W-VAAC advisories are often based on local VONA reports or directly on the webcam heights. Regardless, as depicted in Figure 6, since they report only positive (above crater level) heights and do so in 1000 ft steps, they overestimated very low volcanic plumes and underestimated larger ones, resulting in a weak correlation (a -value = 0.39, $R^2 = 0.30$). Additionally, W-VAAC alerts are generally issued every six hours, unless there are significant changes in activity, which is why height estimates are not always readily available, and tracking eruption conditions in near-real-time solely based on this method is nonviable.

This emphasizes, once again, the importance of relying on multiple sources to improve height estimates and, consequently, the accuracy of hazard communication, as well as input parameters for ash dispersal and deposition modeling.

4.3 Relevance

One of the main sectors to be negatively impacted by ash emissions is aviation, since volcanic ash can severely damage jet engines and even cause engine failure [Guffanti et al. 2010; Clarkson et al. 2016]. The risk is particularly high for domestic and international flights departing from and arriving to Quito airport with southern destination/origin, since they generally pass less than 50 km west of Cotopaxi at approximate altitudes between 5100 and 8700 m asl, corresponding to 800 m bcl and 2800 m acl, respectively [FlightAware 2023]. The low flight altitudes close to Cotopaxi are related to the proximity of Cotopaxi to Quito airport (60 km), due to which airplanes are in their takeoff/landing phase and not at their maximum flight altitude. Considering that for much of the year wind in con-

tinental Ecuador blows from east to west, most flight routes directly cross the area most likely to be affected by volcanic ash during an eruption of Cotopaxi. Therefore, it is extremely important to assess and communicate the presence and height of volcanic ash clouds 24/7 as quickly and accurately as possible. Moreover, much of Ecuadorian economy depends on agriculture, from local businesses to large-scale exportation, and most productive lands are found close to volcanoes, since eruptive material refreshes the soils by adding nutrients and minerals [Calispa et al. 2023]. However, ash fall is also known to severely damage crops and reduce harvests [Wilson and Kaye 2007; Ligot et al. 2022], which is why local and regional fallouts have strong negative impacts on the country's economy. To avoid or at least minimize these adverse impacts, timely communication of possible ash fall in a specific area is crucial, especially when issued in combination with infographics indicating appropriate safety measures to be taken, such as avoiding exposure, using a face mask, sheltering livestock, and covering water tanks.

To do so, it is imperative that staff at volcano observatories constantly perform rapid hazard assessments for all ash emissions recorded during 24/7 volcanic monitoring activities. At IG-EPN, when an ash emission is observed, the priority is to issue a VONA for aviation safety. Then, in case the ash emission seems to be large enough to cause ash fall in populated areas, a special bulletin (IGAllistante) describing the observed ash cloud height, the dispersal direction and the possibly affected regions, as well as what to do to reduce the negative impacts, is published on the IG-EPN webpage and social media accounts and sent directly to civil protection agencies [Bernard et al. 2022]. When direct observations of the volcanoes are not available due to cloudy weather, darkness, or defective/non-existent webcams, satellite imagery is a valuable resource for volcanic monitoring [Bailey et al. 2010; Gordeev et al. 2016; Scollo et al. 2019]. Since there is an inherent delay of 20 to 30 minutes in receiving GOES-16 satellite imagery, it is in the interest of the volcano observatory to reduce any possible further delay when analyzing the images and assessing the possible hazard. Therefore, when readily available, ash cloud height estimates reported by the W-VAAC are used for the VONA and the special bulletins. However, for situations in which that is not the case, the chart in Figure 9 serves as a rapid guide for estimating ash cloud height directly based on the brightness temperature observed on the Color Enhanced Infrared BT imagery and the average atmospheric temperature gradient retrieved from READY sounding files for the three currently active volcanoes in Ecuador.

As shown in Figure 10, in the Ecuadorian Andes the atmospheric temperature gradient does not vary much over the course of the day or during different times of the year. The largest standard deviation (>1.5 degrees) is observed for altitudes above 16.5 km asl, corresponding to rare high (>10 km acl) eruptive plumes. In cases of such high eruptive columns, the atmospheric temperature reversal at the tropopause means multiple heights can correspond to the same temperature, complicating the brightness temperature method. Bailey et al. [2010] suggested assuming the cloud ascended through the tropopause to the height of neutral buoy-

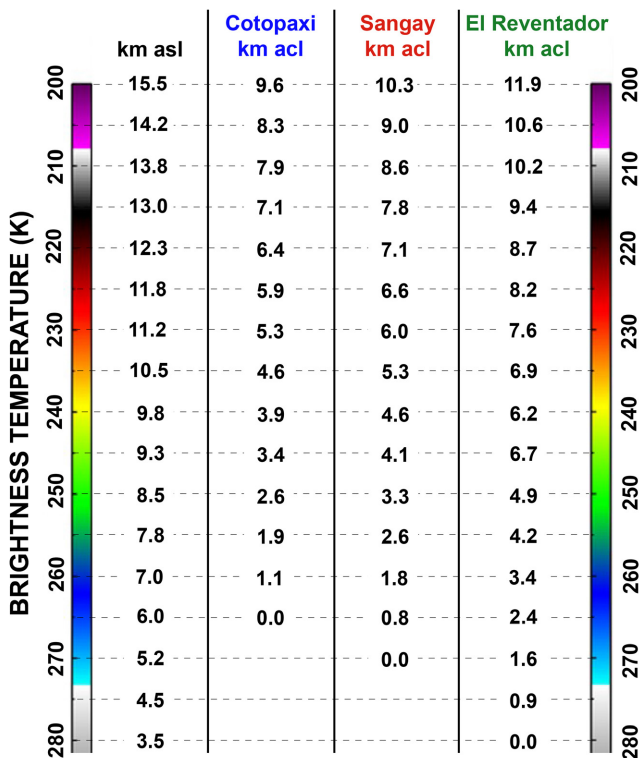


Figure 9: Overview chart for rapid ash cloud height estimation based on the brightness temperature observed in BT imagery provided by NOAA/CIMSS Volcanic Cloud Monitoring Program and the average atmospheric temperature gradient obtained from meteorological models provided by READY.

ancy, matching the recorded temperature at the initial height. Similarly, Guerrieri et al. [2023] always selected the lowest height matching the observed temperature. Estimating and retrieving ash cloud heights from additional sources can further help to constrain the resulting values. For the regularly observed ash plume heights in continental Ecuador (<10 km acl), however, variation lies within or close to one degree, making Figure 9 particularly useful for a rapid ash cloud height estimation based on the ash emission’s brightness temperature. Importantly, since the present analysis has shown that for low (<3 km acl) ash emissions the heights obtained via the brightness temperature systematically fall below the heights observed on camera, the initial analysis performed with the chart in Figure 9 mainly serves to quickly discriminate between small low-impact and moderate to large high-impact emissions, rather than delivering a definite height value. Nevertheless, its accuracy can be improved by applying the 2 K decrease in the obtained brightness temperature for faint volcanic clouds before estimating the corresponding height.

In addition to the rapidly estimated ash cloud height, the observed dispersal direction of a given ash emission is combined with simplified maps, such as the one shown in Figure 11, to immediately read and communicate which towns and regions are likely to be affected by ashfall. Once a timely first warning has been issued and the civil protection authorities have been informed about the ongoing eruption and possible affected ar-

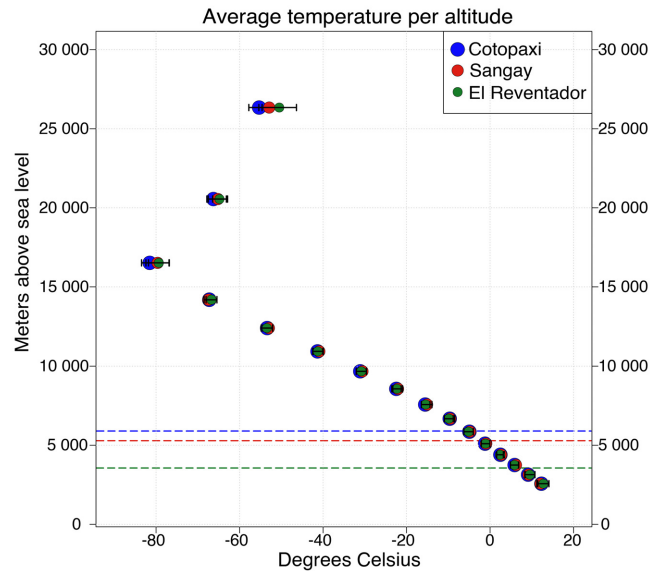


Figure 10: Average temperature per altitude point including standard deviation for 49 Cotopaxi, 43 Sangay, and 23 Reventador GDAS Sounding products collected over multiple months at varying times of the day and night with the respective summit height as reference (dashed lines).

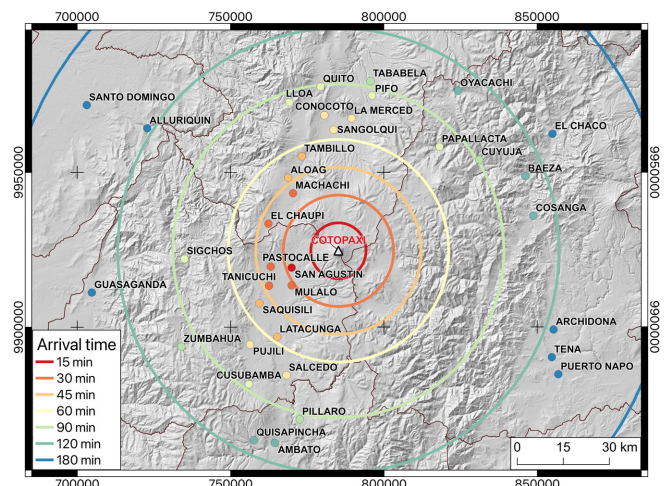


Figure 11: Arrival time of ash clouds to towns assuming an average wind speed of 10 m s⁻¹ (36 km h⁻¹).

eas, time is taken to calculate more exact source parameters and communicate with other entities such as the W-VAAC to get their assessment and height estimates, which can then be used to feed ash dispersion models (such as Ash3D) and be communicated in a follow-up bulletin.

Figure 11 indicates that for a fixed wind speed of 10 m s⁻¹ (36 km h⁻¹), which approximately corresponds to the average ash cloud speeds recorded at Cotopaxi over the past year plus one standard deviation (68 %), most potentially affected towns are more than 30 minutes away (line-of-sight distance) from Cotopaxi. This observation supports the notion that ash fall alerts issued 30 to 40 minutes after an eruption based on satellite imagery remain useful for risk reduction.

5 CONCLUSION

Ash plume height estimates, combined with spreading direction and speed, are crucial parameters for hazard assessment and communication at volcano observatories, especially to inform the civil aviation of ash contamination in the atmosphere and nearby settlements of possible ash fallouts. The most direct source to obtain these parameters are direct visual observations, which are, however, not always available: especially during cloudy days, nighttime, and at remotely located volcanoes. In these cases, satellite imagery analysis is key when assessing the hazard level of an eruption, for forecasting ash dispersion and deposition, and issuing accurate warnings. Our comparison between direct visual observations of ash plume heights and those estimated from the direction and the brightness temperature of the ash clouds in GOES-16 imagery in combination with global meteorological models, as well as heights retrieved from VOLCAT products and those reported in W-VAAC advisories, show that for the latest phase of activity at Cotopaxi volcano (2022–2023) most satellite-based ash cloud height estimates fall below those observed on webcam. In part, this is possibly because webcam heights are maximum eruptive column values recorded just above the volcano, while satellite height estimates represent the spreading and dispersion height of the ash clouds over a larger area. Moreover, we find that W-VAAC advisories and the plume direction method produce, on average, the closest approximations to visual observations. However, they also exhibit significant deviations. Conversely, while the temperature-based method yields the lowest ash cloud heights, it presents the best linear regression with webcam heights. In addition, it demonstrates temporal and spatial stability, as well as decreasing underestimation with increasing eruption size, which positions this method as a useful discriminator between small low-impact and moderate to large volcanic ash emissions. This discrimination is crucial at volcano observatories for a first timely hazard assessment and communication done during 24/7 monitoring of active volcanoes. Furthermore, the large scatter in height estimates underscores the importance of relying on more than one source to constrain the most likely ash cloud height. Improving the direction and temperature-based methods by using local high-resolution meteorological models could serve to obtain more accurate ash cloud height estimates, which are, in turn, crucial for hazard communication and forecasting volcanic ash dispersion and fallout.

AUTHOR CONTRIBUTIONS

BB developed the methodology presented in this manuscript. AVM retrieved the heights of ash clouds observed on GOES-16 satellite imagery and FJV those captured on webcams for Cotopaxi between October 2022 and July 2023. AVM conducted the data analysis and FJV produced the figures. AVM wrote the manuscript and BB and FJV reviewed and improved it.

ACKNOWLEDGEMENTS

The authors would like to thank the dedicated staff of the IG-EPN for their ongoing vigilance in monitoring Ecuadorian volcanoes and ensuring the operational status of the webcam network around Cotopaxi, without which this study would

not have been possible. We also thank the Washington VAAC team for their assistance and cooperation throughout this last eruptive phase of Cotopaxi and especially Jamie Kibler and the VOLCAT group for providing us with the satellite imagery presented in this article.

DATA AVAILABILITY

Supporting information is available alongside the online version of this manuscript. **Supplementary Material 1:** Spreadsheet containing the formulas presented in this article and **Supplementary Material 2:** Webcam videos and photographs of Cotopaxi's ash emissions. **Supplementary Material 3:** Ash cloud heights obtained via the six different methods plotted against each other.

COPYRIGHT NOTICE

© The Author(s) 2024. This article is distributed under the terms of the **Creative Commons Attribution 4.0 International License**, which permits unrestricted use, distribution, and reproduction in any medium, provided you give appropriate credit to the original author(s) and the source, provide a link to the Creative Commons license, and indicate if changes were made.

REFERENCES

- Aubry, T. J., S. L. Engwell, C. Bonadonna, L. G. Mastin, G. Carazzo, A. R. Van Eaton, D. E. Jessop, R. G. Grainger, S. Scollo, I. A. Taylor, A. M. Jellinek, A. Schmidt, S. Biass, and M. Gouhier (2023). “New Insights Into the Relationship Between Mass Eruption Rate and Volcanic Column Height Based On the IVESPA Data Set”. *Geophysical Research Letters* 50(14), e2022GL102633. DOI: [10.1029/2022GL102633](https://doi.org/10.1029/2022GL102633).
- Bailey, J. E., K. G. Dean, J. Dehn, and P. W. Webley (2010). *Integrated satellite observations of the 2006 eruption of Augustine Volcano*. The 2006 Eruption of Augustine Volcano, Alaska 1769–20. USGS Publications Warehouse, pages 481–506. DOI: [10.3133/pp176920](https://doi.org/10.3133/pp176920).
- Barberi, F., M. Coltelli, A. Frullani, M. Rosi, and E. Almeida (1995). “Chronology and dispersal characteristics of recently (last 5000 years) erupted tephra of Cotopaxi (Ecuador): Implications for long-term eruptive forecasting”. *Journal of Volcanology and Geothermal Research* 69(3–4), pages 217–239. DOI: [10.1016/0377-0273\(95\)00017-8](https://doi.org/10.1016/0377-0273(95)00017-8).
- Barnie, T., T. Hjörvar, M. Titos, E. M. Sigurðsson, S. K. Pálsson, B. Bergsson, Þ. Ingvarsson, M. A. Pfeffer, S. Barsotti, Þ. Arason, V. S. Þorvaldsson, S. Von Löwis Of Menar, and B. Oddsson (2023). “Volcanic plume height monitoring using calibrated web cameras at the Icelandic Meteorological Office: System overview and first application during the 2021 Fagradalsfjall eruption”. *Journal of Applied Volcanology* 12(1), page 4. DOI: [10.1186/s13617-023-00130-9](https://doi.org/10.1186/s13617-023-00130-9).
- Barsotti, S., D. Andronico, A. Neri, P. Del Carlo, P. J. Baxter, W. P. Aspinall, and T. Hincks (2010). “Quantitative assessment of volcanic ash hazards for health and infrastructure at Mt. Etna (Italy) by numerical simulation”. *Journal of Volcanology and Geothermal Research* 192(1), pages 85–96. DOI: [10.1016/j.jvolgeores.2010.02.011](https://doi.org/10.1016/j.jvolgeores.2010.02.011).

- Beckett, F. M., D. Bensimon, A. Crawford, M. Deslandes, V. Guidard, M. C. Hort, M. Jeoffrion, N. Kristiansen, C. Lucas, A. Nishijo, S. Osoreo, E. Renard, G. Servranckx, E. Snee, R. Trancoso, and E. Vazquez (2024). “VAAC Model Setup Tables 2023”. *Zenodo*. DOI: [10.5281/zenodo.10671098](https://doi.org/10.5281/zenodo.10671098). [Dataset].
- Bernard, B., J. Battaglia, A. Proaño, S. Hidalgo, F. Vásconez, S. Hernandez, and M. Ruiz (2016). “Relationship between volcanic ash fallouts and seismic tremor: Quantitative assessment of the 2015 eruptive period at Cotopaxi volcano, Ecuador”. *Bulletin of Volcanology* 78(11), page 80. DOI: [10.1007/s00445-016-1077-5](https://doi.org/10.1007/s00445-016-1077-5).
- Bernard, B., P. Samaniego, L. Mastin, S. Hernandez, G. Pino, J. Kibler, M. Encalada, S. Hidalgo, and N. Vizuete (2022). “Forecasting and communicating the dispersion and fallout of ash during volcanic eruptions: Lessons from the September 20, 2020 eruptive pulse at Sangay volcano, Ecuador”. *Frontiers in Earth Science* 10, page 912835. DOI: [10.3389/feart.2022.912835](https://doi.org/10.3389/feart.2022.912835).
- Blake, D. M., T. M. Wilson, J. W. Cole, N. I. Deligne, and J. M. Lindsay (2017). “Impact of Volcanic Ash on Road and Airfield Surface Skid Resistance”. *Sustainability* 9(8), Article 8. DOI: [10.3390/su9081389](https://doi.org/10.3390/su9081389).
- Bonadonna, C., A. Costa, A. Folch, and T. Koyaguchi (2015). “Tephra Dispersal and Sedimentation”. *The Encyclopedia of Volcanoes*. Edited by B. Houghton, S. McNutt, H. Rymer, and J. Stix. Elsevier, pages 587–597.
- Calispa, M., F. Vasconez, S. Santamaría, and P. Samaniego (2023). “Los suelos de los páramos del Ecuador”. *Los páramos del Ecuador: Pasado, presente y futuro*. USFQ Press, page 36.
- Calvari, S., G. G. Salerno, L. Spampinato, M. Gouhier, A. La Spina, E. Pecora, A. J. L. Harris, P. Labazuy, E. Biale, and E. Boschi (2011). “An unloading foam model to constrain Etna’s 11-13 January 2011 lava fountaining episode”. *Journal of Geophysical Research: Solid Earth* 116(B11). DOI: [10.1029/2011JB008407](https://doi.org/10.1029/2011JB008407).
- Cas, R. and J. V. Wright (1996). *Volcanic successions: Modern and ancient; a geological approach to processes, products and successions*. Chapman & Hall.
- Clarkson, R. J., E. J. Majewicz, and P. Mack (2016). “A re-evaluation of the 2010 quantitative understanding of the effects volcanic ash has on gas turbine engines”. *Proceedings of the Institution of Mechanical Engineers, Part G: Journal of Aerospace Engineering* 230(12), pages 2274–2291.
- Corradini, S., M. Montopoli, L. Guerrieri, M. Ricci, S. Scollo, L. Merucci, F. Marzano, S. Pugnaghi, M. Prestifilippo, L. Ventress, R. Grainger, E. Carboni, G. Vulpiani, and M. Coltelli (2016). “A Multi-Sensor Approach for Volcanic Ash Cloud Retrieval and Eruption Characterization: The 23 November 2013 Etna Lava Fountain”. *Remote Sensing* 8(1), page 58. DOI: [10.3390/rs8010058](https://doi.org/10.3390/rs8010058).
- Degruyter, W. and C. Bonadonna (2012). “Improving on mass flow rate estimates of volcanic eruptions”. *Geophysical Research Letters* 39(16). DOI: [10.1029/2012GL052566](https://doi.org/10.1029/2012GL052566).
- Dioguardi, F., F. Beckett, T. Dürig, and J. A. Stevenson (2020). “The Impact of Eruption Source Parameter Uncertainties on Ash Dispersion Forecasts During Explosive Volcanic Eruptions”. *Journal of Geophysical Research: Atmospheres* 125(17), e2020JD032717. DOI: [10.1029/2020JD032717](https://doi.org/10.1029/2020JD032717).
- FlightAware (2023). *FlightAware*. URL: <http://www.flightaware.com/> (visited on 06/18/2024).
- Folch, A., A. Costa, and S. Basart (2012). “Validation of the FALL3D ash dispersion model using observations of the 2010 Eyjafjallajökull volcanic ash clouds”. *Atmospheric Environment* 48, pages 165–183. DOI: [10.1016/j.atmosenv.2011.06.072](https://doi.org/10.1016/j.atmosenv.2011.06.072).
- Gordeev, E. I., O. A. Girina, E. A. Lupyan, A. A. Sorokin, L. S. Kramareva, V. Y. Efremov, A. V. Kashnitskii, I. A. Uvarov, M. A. Burtsev, I. M. Romanova, D. V. Mel’nikov, A. G. Manevich, S. P. Korolev, and A. L. Verkhoturov (2016). “The VolSatView information system for Monitoring the Volcanic Activity in Kamchatka and on the Kuril Islands”. *Journal of Volcanology and Seismology* 10(6), pages 382–394. DOI: [10.1134/S074204631606004X](https://doi.org/10.1134/S074204631606004X).
- Guerrieri, L., S. Corradini, N. Theys, D. Stelitano, and L. Merucci (2023). “Volcanic Clouds Characterization of the 2020–2022 Sequence of Mt. Etna Lava Fountains Using MSG-SEVIRI and Products’ Cross-Comparison”. *Remote Sensing* 15(8), page 2055. DOI: [10.3390/rs15082055](https://doi.org/10.3390/rs15082055).
- Guffanti, M., T. J. Casadevall, and K. E. Budding (2010). *Encounters of aircraft with volcanic ash clouds: A compilation of known incidents, 1953-2009*. US Department of Interior, US Geological Survey.
- Hall, M. and P. Mothes (2008). “The rhyolitic–andesitic eruptive history of Cotopaxi volcano, Ecuador”. *Bulletin of Volcanology* 70(6), pages 675–702. DOI: [10.1007/s00445-007-0161-2](https://doi.org/10.1007/s00445-007-0161-2).
- Hidalgo, S., F. J. Vasconez, J. Battaglia, B. Bernard, P. Espín, S. Valade, M.-F. Naranjo, R. Campion, J. Salgado, M. Córdova, M. Almeida, S. Hernández, G. Pino, E. Gaunt, A. Bell, P. Mothes, and M. Ruiz (2022). “Sangay volcano (Ecuador): The opening of two new vents, a drumbeat seismic sequence and a new lava flow in late 2021”. *Volcanica* 5(2), pages 295–311. DOI: [10.30909/vol.05.02.295311](https://doi.org/10.30909/vol.05.02.295311).
- Jenkins, S. F., T. Wilson, C. Magill, V. Miller, C. Stewart, R. Blong, and W. Marzocchi (2015). “Volcanic ash fall hazard and risk”. *Global volcanic hazards and risk*. Edited by M. Boulton, C. Bonadonna, and A. Costa. Cambridge University Press, pages 173–221. DOI: [10.1017/CB09781316276273.005](https://doi.org/10.1017/CB09781316276273.005).
- Ligot, N., P. Bogaert, S. Biass, G. Lobet, and P. Delmelle (2023). “Grain size modulates volcanic ash retention on crop foliage and potential yield loss”. *Natural Hazards and Earth System Sciences* 23(4), pages 1355–1369. DOI: [10.5194/nhess-23-1355-2023](https://doi.org/10.5194/nhess-23-1355-2023).
- Ligot, N., A. Guevara, and P. Delmelle (2022). “Drivers of crop impacts from tephra fallout: Insights from interviews with farming communities around Tungurahua volcano, Ecuador”. *Volcanica* 5(1), pages 163–181. DOI: [10.30909/vol.05.01.163181](https://doi.org/10.30909/vol.05.01.163181).
- Marzano, F. S., L. Mereu, S. Scollo, F. Donnadieu, and C. Bonadonna (2020). “Tephra Mass Eruption Rate From Ground-Based X-Band and L-Band Microwave Radars During the November 23, 2013, Etna Paroxysm”. *IEEE Transactions on Geoscience and Remote Sensing* 58(5), pages 3314–3327. DOI: [10.1109/TGRS.2019.2953167](https://doi.org/10.1109/TGRS.2019.2953167).

- Mastin, L. G. (2014). “Testing the accuracy of a 1-D volcanic plume model in estimating mass eruption rate”. *Journal of Geophysical Research: Atmospheres* 119(5), pages 2474–2495. DOI: [10.1002/2013JD020604](https://doi.org/10.1002/2013JD020604).
- Mastin, L. G., M. Guffanti, R. Servranckx, P. Webley, S. Barsotti, K. Dean, A. Durant, J. W. Ewert, A. Neri, W. I. Rose, D. Schneider, L. Siebert, B. Stunder, G. Swanson, A. Tupper, A. Volentik, and C. F. Waythomas (2009). “A multidisciplinary effort to assign realistic source parameters to models of volcanic ash-cloud transport and dispersion during eruptions”. *Journal of Volcanology and Geothermal Research* 186(1), pages 10–21. DOI: [10.1016/j.jvolgeores.2009.01.008](https://doi.org/10.1016/j.jvolgeores.2009.01.008).
- Mastin, L. G., M. J. Randall, H. F. Schwaiger, and R. P. Denlinger (2013). *User’s guide and reference to Ash3d—A three-dimensional model for Eulerian atmospheric tephra transport and deposition*. Open-File Report 2013–1122, page 25. DOI: [10.3133/ofr20131122](https://doi.org/10.3133/ofr20131122).
- Mereu, L., S. Scollo, A. Garcia, L. Sandri, C. Bonadonna, and F. S. Marzano (2023). “A New Radar-Based Statistical Model to Quantify Mass Eruption Rate of Volcanic Plumes”. *Geophysical Research Letters* 50(7), e2022GL100596. DOI: [10.1029/2022GL100596](https://doi.org/10.1029/2022GL100596).
- Osman, S., M. Thomas, J. Crummy, and S. Carver (2022). “Investigation of geomechanical properties of tephra relevant to roof loading for application in vulnerability analyses”. *Journal of Applied Volcanology* 11(1), page 9. DOI: [10.1186/s13617-022-00121-2](https://doi.org/10.1186/s13617-022-00121-2).
- Pavolonis, M. J., J. Sieglaff, and J. Cintineo (2018). “Automated Detection of Explosive Volcanic Eruptions Using Satellite-Derived Cloud Vertical Growth Rates”. *Earth and Space Science* 5(12), pages 903–928. DOI: [10.1029/2018EA000410](https://doi.org/10.1029/2018EA000410).
- (2015a). “Spectrally Enhanced Cloud Objects—A generalized framework for automated detection of volcanic ash and dust clouds using passive satellite measurements: 1. Multispectral analysis”. *Journal of Geophysical Research: Atmospheres* 120(15), pages 7813–7841. DOI: [10.1002/2014JD022968](https://doi.org/10.1002/2014JD022968).
- (2015b). “Spectrally Enhanced Cloud Objects—A generalized framework for automated detection of volcanic ash and dust clouds using passive satellite measurements: 2. Cloud object analysis and global application”. *Journal of Geophysical Research: Atmospheres* 120(15), pages 7842–7870. DOI: [10.1002/2014JD022969](https://doi.org/10.1002/2014JD022969).
- Prata, A. J. and I. F. Grant (2001). “Retrieval of microphysical and morphological properties of volcanic ash plumes from satellite data: Application to Mt Ruapehu, New Zealand”. *Quarterly Journal of the Royal Meteorological Society* 127(576), pages 2153–2179. DOI: [10.1002/qj.49712757615](https://doi.org/10.1002/qj.49712757615).
- Ramírez, J., F. J. Vasconez, A. López, F. Valencia, F. Quilumba, A. Vasconez Müller, S. Hidalgo, and B. Bernard (2022). “Impact of volcanic ash from Cotopaxi-2015 and Tungurahua-2016 eruptions on the dielectric characteristics of suspension insulators, Ecuador”. *Journal of Applied Volcanology* 11(1), page 7. DOI: [10.1186/s13617-022-00117-y](https://doi.org/10.1186/s13617-022-00117-y).
- Rolph, G., A. Stein, and B. Stunder (2017). “Real-time Environmental Applications and Display sYstem: READY”. *Environmental Modelling & Software* 95, pages 210–228. DOI: [10.1016/j.envsoft.2017.06.025](https://doi.org/10.1016/j.envsoft.2017.06.025).
- Scollo, S., M. Prestifilippo, C. Bonadonna, R. Cioni, S. Corradini, W. Degruyter, E. Rossi, M. Silvestri, E. Biale, G. Carparelli, C. Cassisi, L. Merucci, M. Musacchio, and E. Pecora (2019). “Near-Real-Time Tephra Fallout Assessment at Mt. Etna, Italy”. *Remote Sensing* 11(24), page 2987. DOI: [10.3390/rs11242987](https://doi.org/10.3390/rs11242987).
- Simpson, J., G. Hufford, D. Pieri, and J. Berg (2000). “Failures in Detecting Volcanic Ash from a Satellite-Based Technique”. *Remote Sensing of Environment* 72(2), pages 191–217. DOI: [10.1016/S0034-4257\(99\)00103-0](https://doi.org/10.1016/S0034-4257(99)00103-0).
- Simpson, J., G. L. Hufford, D. Pieri, and J. S. Berg (2001). “Response to ‘Comments on ‘Failures in detecting volcanic ash from a satellite-based technique.’”” *Remote Sensing of Environment* 78(3), pages 347–357. DOI: [10.1016/S0034-4257\(01\)00230-9](https://doi.org/10.1016/S0034-4257(01)00230-9).
- Snee, E., P. A. Jarvis, R. Simionato, S. Scollo, M. Prestifilippo, W. Degruyter, and C. Bonadonna (2023). “Image analysis of volcanic plumes: A simple calibration tool to correct for the effect of wind”. *Volcanica* 6(2), pages 447–458. DOI: [10.30909/vol.06.02.447458](https://doi.org/10.30909/vol.06.02.447458).
- Sodiro, L. (1877). *Relacion sobre la erupcion del Cotopaxi acaecida del dia 26 de junio, 1877*. Imprenta Nacional Quito.
- Stewart, C., D. E. Damby, C. J. Horwell, T. Elias, E. Ilyinskaya, I. Tomašek, B. M. Longo, A. Schmidt, H. K. Carlsen, E. Mason, P. J. Baxter, S. Cronin, and C. Witham (2022). “Volcanic air pollution and human health: Recent advances and future directions”. *Bulletin of Volcanology* 84(1), page 11. DOI: [10.1007/s00445-021-01513-9](https://doi.org/10.1007/s00445-021-01513-9).
- Tupper, A., I. Itikarai, M. Richards, F. Prata, S. Carn, and D. Rosenfeld (2007). “Facing the Challenges of the International Airways Volcano Watch: The 2004/05 Eruptions of Manam, Papua New Guinea”. *Weather and Forecasting* 22(1), pages 175–191. DOI: [10.1175/WAF974.1](https://doi.org/10.1175/WAF974.1).
- Webley, P. W., J. Dehn, J. Lovick, K. G. Dean, J. E. Bailey, and L. Valcic (2009). “Near-real-time volcanic ash cloud detection: Experiences from the Alaska Volcano Observatory”. *Journal of Volcanology and Geothermal Research* 186(1–2), pages 79–90. DOI: [10.1016/j.jvolgeores.2009.02.010](https://doi.org/10.1016/j.jvolgeores.2009.02.010).
- Wilson, G., T. Wilson, N. I. Deligne, and J. W. Cole (2014). “Volcanic hazard impacts to critical infrastructure: A review”. *Journal of Volcanology and Geothermal Research* 286, pages 148–182. DOI: [10.1016/j.jvolgeores.2014.08.030](https://doi.org/10.1016/j.jvolgeores.2014.08.030).
- Wilson, T. and G. D. Kaye (2007). “Agricultural fragility estimates for volcanic ash fall hazards”. *GNS Science report 2007 (37)*. Institute of Geological and Nuclear Sciences, New Zealand.
- Wilson, T., C. Stewart, V. Sword-Daniels, G. S. Leonard, D. M. Johnston, J. W. Cole, J. Wardman, G. Wilson, and S. T. Barnard (2012). “Volcanic ash impacts on critical infrastructure”. *Physics and Chemistry of the Earth, Parts a/b/c* 45, pages 5–23. DOI: <https://doi.org/10.1016/j.pce.2011.06.006>.